Spin $I = 1$ NMR Patterns for the Case of Twofold Internal Spin Interactions

B. Boddenberg and G. Neue

Lehrstuhl für Physikalische Chemie II, Universität Dortmund

Z. Naturforsch. **42a**, 948–956 (1987); received April 3, 1987

An operator formalism is developed which allows a convenient calculation of high field spin $I = 1$ solid state NMR powder spectra for the case that the spins are acted on not only electrically via an electric field gradient tensor but also magnetically via a shielding tensor. Examples of practical applications in the field of surface science are given.

I. Introduction

Solid state NMR spectra are, in general, dominated by one type of internal spin interaction, dipolar for spin $I = 1/2$ and quadrupolar for spin $I > 1/2$ nuclei. Most recently, however, it was observed [1] that deuterons (spin $I = 1$) being contained in molecules adsorbed on the basal planes of graphite in addition to the coupling with the electric field gradient (EFG) tensor experience an anisotropic magnetic shielding (S) which is caused by the polarization in the strong Zeeman field of the graphite support due to its unusually large diamagnetic susceptibility anisotropy. This magnetic coupling shows up in characteristic asymmetries of the powder patterns determined experimentally. Asymmetries of similar types for spin $I = 1$ nuclei (^{2}H, ^{14}N) have recently been observed in lipid bilayers in the presence of paramagnetic ions [2]. In these cases it is the motionally averaged dipolar coupling between the resonant spins and the spins of the paramagnetic species which competes for dominance with the quadrupolar interaction.

Although the calculation of powder patterns in the case of axially symmetric EFG and S tensors at any given relative orientation of the tensor principle axis coordinate (PAS) frames is straightforward [1] the rather tedious computational work encountered as well as the desire to cover the cases of non axially symmetric tensors requires a more convenient treatment of the problem. This task is undertaken in the present paper.

Reprint requests to Prof. Dr. B. Boddenberg, Lehrstuhl für Physikalische Chemie II, Universität Dortmund, Postfach 500500, D-4600 Dortmund 50.

II. Operator Basis Set and Nuclear Spin Hamiltonian

A set of eight linearly independent traceless Hermitian operators appropriate for the treatment of an ensemble of noninteracting like spins $I = 1$ in an external magnetic field B_0 is introduced as

$$\begin{aligned} L_z^{10} &= \tfrac{1}{2}(I_z^2 + I_z) - \tfrac{1}{6}I^2 \,, \\ L_z^{0-1} &= -\tfrac{1}{2}(I_z^2 - I_z) + \tfrac{1}{6}I^2 \,. \end{aligned} \tag{1}$$

The operators L_x^{10}, L_x^{0-1}, L_x^{1-1}, L_y^{10}, L_y^{0-1}, and L_y^{1-1} which complete L_z^{10} and L_z^{0-1} to an operator basis set [3] are chosen identical with the single transition operators $I_x^{(12)}$, $I_x^{(23)}$, $I_x^{(13)}$, $I_y^{(12)}$, $I_y^{(23)}$, and $I_y^{(13)}$, respectively, introduced by Wokaun and Ernst [4]. The matrix representation of this operator base in the eigenfunction base of I_z, $\{|1\rangle, |0\rangle, |-1\rangle\}$, is given in Table 1.

The operators just defined obey standard angular momentum commutation relations such as

$$[L_z^{10}, L_z^{0-1}] = 0 \,, \tag{2}$$

$$[L_z^{\mathrm{rs}}, L_x^{\mathrm{st}}] = [L_z^{\mathrm{rs}}, L_y^{\mathrm{st}}] = 0 \,, \tag{3}$$

$$\begin{aligned} [L_z^{\mathrm{rs}}, L_x^{\mathrm{rs}}] &= iL_y^{\mathrm{rs}} \,, \\ [L_z^{\mathrm{rs}}, L_y^{\mathrm{rs}}] &= -iL_x^{\mathrm{rs}} \,. \end{aligned} \tag{4}$$

Two prominent properties of the base operators which are of importance in the following become apparent from an inspection of the matrices in Table 1. L_z^{10} has those diagonal elements equal which are obtained from the states carrying the same labels as L_z^{0-1}, and vice versa. L_x^{10}, L_x^{0-1}, L_y^{10}, and L_y^{0-1}, on the other hand, just connect the states which appear as labels of these operators. Thus, they connect the states having different eigenvalues of L_z^{10} and L_z^{0-1}.

0932-0784 / 87 / 0900-0948 $ 01.30/0. – Please order a reprint rather than making your own copy.

The nuclear spin operator components I_x, I_y, and I_z may be expressed in terms of the base operators as

$$I_x = \frac{1}{\sqrt{2}}(L_x^{10} + L_x^{0-1}) \ ,$$
$$I_y = \frac{1}{\sqrt{2}}(L_y^{10} + L_y^{0-1}) \ , \tag{5}$$
$$I_z = L_z^{10} + L_z^{0-1} \ .$$

The secular part of the nuclear spin Hamiltonian, $\mathscr{H}$, of a spin $I = 1$ nucleus which besides the Zeeman (Z) coupling in a strong static magnetic field B_0 experiences an electric quadrupole (Q) and a magnetic shielding (S) coupling may be written as (in units h)

$$\mathscr{H} = -\nu_0 I_z + \nu_Q (I_z^2 - \tfrac{1}{3} I^2) + \nu_S I_z \ , \tag{6}$$

where ν_0 and ν_Q, ν_S are the laboratory (L) frame zz components of zero rank and traceless symmetric second rank tensors $\boldsymbol{\nu}_0$ and $\boldsymbol{\nu}_Q$, $\boldsymbol{\nu}_S$, respectively. The Cartesian representations of these tensors are [5]

$$\boldsymbol{\nu}_0 = \nu_Z (1 - s_0) \begin{pmatrix} 1 & 0 & 0 \\ 0 & 1 & 0 \\ 0 & 0 & 1 \end{pmatrix} \tag{7}$$

and, in their respective principal axis (PAS) frames, which are the PAS's of the EFG and S tensors,

$$\boldsymbol{\nu}_Q = \tfrac{3}{4}\,\mathrm{QCC} \begin{pmatrix} -\frac{1}{2}(1+\eta_Q) & 0 & 0 \\ 0 & -\frac{1}{2}(1-\eta_Q) & 0 \\ 0 & 0 & 1 \end{pmatrix} , \tag{8}$$

$$\boldsymbol{\nu}_S = \tfrac{2}{3}\,\nu_Z \Delta s \begin{pmatrix} -\frac{1}{2}(1+\eta_S) & 0 & 0 \\ 0 & -\frac{1}{2}(1-\eta_S) & 0 \\ 0 & 0 & 1 \end{pmatrix} . \tag{9}$$

In (7) to (9) $\nu_Z = \gamma_I B_0$ with γ_I the gyromagnetic ratio of the nucleus; s_0 is the isotropic shielding constant and Δs the shielding anisotropy; QCC = $e^2 qQ/h$ is the quadrupole coupling constant; η_Q and η_S are, respectively, the EFG and S tensor asymmetry parameters.

Introducing the previously defined base operators, (6) may be rewritten as

$$\mathscr{H} = -\nu_{10} L_z^{10} - \nu_{0-1} L_z^{0-1} \tag{10}$$

with

$$\nu_{10} = \nu_0 - (\nu_Q + \nu_S) \ ,$$
$$\nu_{0-1} = \nu_0 + (\nu_Q - \nu_S) \ , \tag{11}$$

where $\nu_0 = \nu_Z (1 - s_0)$.

According to (10) and the properties of L_z^{10} and L_z^{0-1} discussed previously the spin $I = 1$ energy level system may be considered separable into two independent fictitious sublevel systems in which the transitions $|1\rangle \rightarrow |0\rangle$ and $|0\rangle \rightarrow |-1\rangle$ with frequencies ν_{10} and ν_{0-1} can be viewed separately (Figure 1). The correctness of the level connections shown in Fig. 1 for the case of a single quantum coherence experiment using a non-selective pulse with

$$\mathscr{H}_{RF} = 2B_1 \cos(2\pi\nu_0 t + \phi) I_x$$
$$= \sqrt{2}\, B_1 \cos(2\pi\nu_0 t + \phi)(L_x^{10} + L_x^{0-1}) \tag{12}$$

can easily be proven with the properties of the L_x operators discussed before.

III. Calculation of NMR Powder Patterns

The frequencies defined in (11) may be considered as the L frame zz-components of the tensors

$$\boldsymbol{\nu}_{10} = \boldsymbol{\nu}_0 - (\boldsymbol{\nu}_Q + \boldsymbol{\nu}_S) \ ,$$
$$\boldsymbol{\nu}_{0-1} = \boldsymbol{\nu}_0 + (\boldsymbol{\nu}_Q - \boldsymbol{\nu}_S) \ , \tag{13}$$

which like their constituents are symmetric and, hence, can be diagonalized. The diagonal elements of the diagonalized Cartesian tensors, i.e. the components of $\boldsymbol{\nu}_{10}$ and $\boldsymbol{\nu}_{0-1}$ in their respective PAS frames (X, Y, Z), can immediately be identified with the distinct frequencies of the shielding type powder patterns [5] which after superposition yield the complete spectrum (Figure 2).

In order to carry out the diagonalization a coordinate frame must be chosen in which both $\boldsymbol{\nu}_Q$ and $\boldsymbol{\nu}_S$ are to be expressed (the rotationally invariant zero rank tensor need not be considered). Since in most cases of interest the quadrupole coupling is dominating the EFG principal axis frame (Q) is conveniently chosen for this purpose. Denoting by $\tilde{\nu}_S^{xx}$, $\tilde{\nu}_S^{xy}$, etc. the Q frame Cartesian components of the reduced tensor $\boldsymbol{\nu}_S / \frac{2}{3}\nu_Z \Delta s$ which by a real orthogonal rotation transformation with Eulerian angles α, β, γ can be obtained

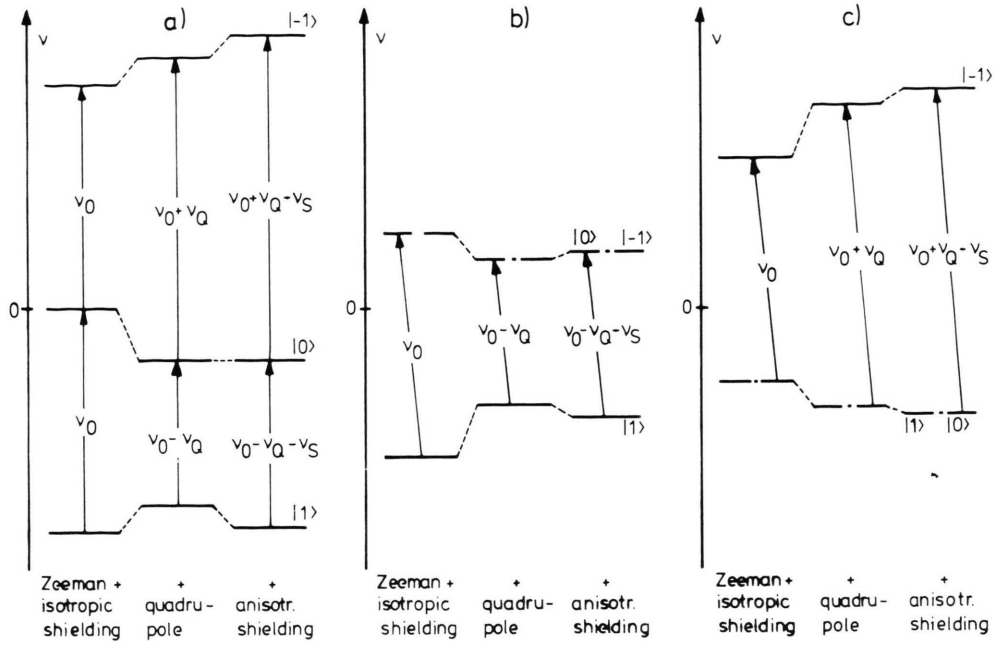

Fig. 1. a) Schematic energy level system and single quantum transitions for a spin $I = 1$ nucleus subject to electric quadrupole and magnetic shielding interactions. b) and c) Fictitious energy level systems with single quantum transitions as described in the text.

[5] from (9) the second rank constituents of ν_{10} and ν_{0-1} come out as

$$\nu_Q \pm \nu_S = \frac{3}{4}\,\mathrm{QCC}\begin{pmatrix} -\frac{1}{2}(1+\eta_Q) \pm A\,\tilde{\nu}_S^{xx} & +A\,\tilde{\nu}_S^{xy} & +A\,\tilde{\nu}_S^{xz} \\ \pm A\,\tilde{\nu}_S^{xz} & -\frac{1}{2}(1-\eta_Q) \pm A\,\tilde{\nu}_S^{yy} & \pm A\,\tilde{\nu}_S^{yz} \\ \pm A\,\tilde{\nu}_S^{xz} & \pm A\,\tilde{\nu}_S^{yz} & 1 \pm A\,\tilde{\nu}_S^{zz} \end{pmatrix} \tag{14}$$

$$\text{with} \quad A = \frac{8}{9}\,\frac{\nu_Z \Delta s}{\mathrm{QCC}} \,. \tag{15}$$

The quantities $\tilde{\nu}_S^{xx}$, $\tilde{\nu}_S^{xy}$, etc. as functions of the Eulerian angles α, β, γ may be found in the literature [5].

Denoting the eigenvalues of $(\nu_Q \pm \nu_S)/\frac{3}{4}\,\mathrm{QCC}$ by $\tilde{\nu}^+(X)$, $\tilde{\nu}^+(Y)$, and $\tilde{\nu}^+(Z)$ such that $|\tilde{\nu}^+(Y)| \leqq |\tilde{\nu}^+(X)| \leqq |\tilde{\nu}^+(Z)|$, the distinct powder pattern frequencies (Fig. 2) are obtained as

$$\begin{aligned} \nu_{10}(X, Y, Z) &= \nu_0 - \tfrac{3}{4}\,\mathrm{QCC}\,\tilde{\nu}^+(X, Y, Z) \,, \\ \nu_{0-1}(X, Y, Z) &= \nu_0 + \tfrac{3}{4}\,\mathrm{QCC}\,\tilde{\nu}^-(X, Y, Z) \,. \end{aligned} \tag{16}$$

Knowing these principal axis frequencies the powder pattern shapes can be calculated by standard procedures [6] and the complete spectrum obtained by additive superposition.

Sometimes it is convenient to characterize the tensors defined in (13) in their respective PAS frame Cartesian representations in the form [7]

$$\left.\begin{matrix} \boldsymbol{\nu}_{10} \\ \boldsymbol{\nu}_{0-1} \end{matrix}\right\} = \nu_0 \begin{pmatrix} 1 & 0 & 0 \\ 0 & 1 & 0 \\ 0 & 0 & 1 \end{pmatrix} + \delta^{\pm} \begin{pmatrix} -\frac{1}{2}(1+\eta^{\pm}) & & 0 \\ 0 & -\frac{1}{2}(1-\eta^{\pm}) & 0 \\ 0 & 0 & 1 \end{pmatrix} \,, \tag{17}$$

where, by definition,

$$\left.\begin{matrix} \delta^+ \\ \delta^- \end{matrix}\right\} = \begin{cases} \nu_{10}(Z) - \frac{1}{3}\,\mathrm{Tr}(\boldsymbol{\nu}_{10}) \,, \\ \nu_{0-1}(Z) - \frac{1}{3}\,\mathrm{Tr}(\boldsymbol{\nu}_{0-1}) \,, \end{cases} \tag{18}$$

and

$$\left.\begin{matrix} \eta^+ \\ \eta^- \end{matrix}\right\} = \begin{cases} [\nu_{10}(Y) - \nu_{10}(X)]/\delta^+ \,, \\ [\nu_{0-1}(Y) - \nu_{0-1}(X)]/\delta^- \,. \end{cases} \tag{19}$$

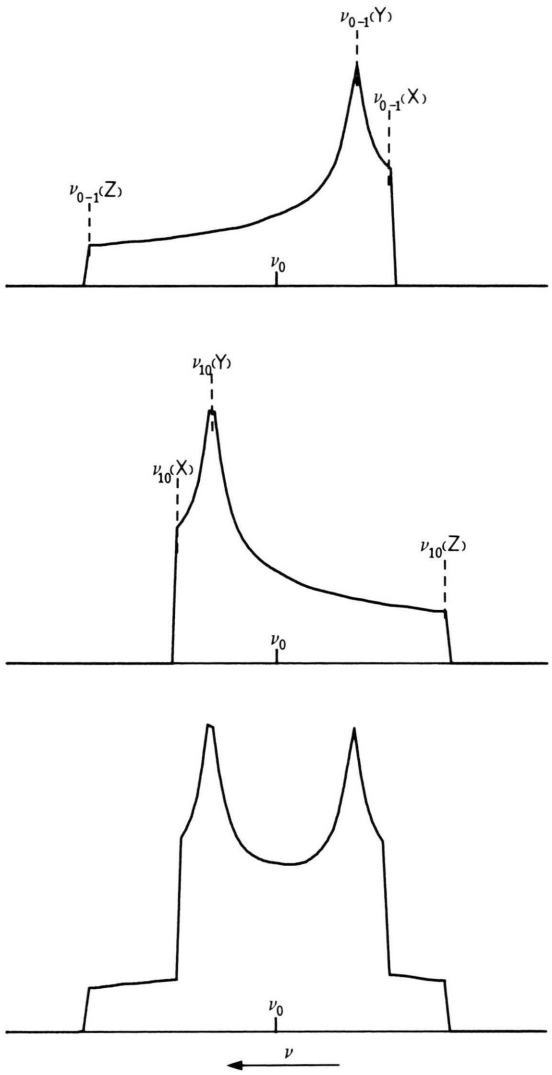

Fig. 2. Schematic powder patterns showing the positions of the principle axis value of the tensors ν_{10} and ν_{0-1}, (13). The spectrum at the bottom is the superposition of the separate shielding type powder patterns.

$\eta^{\pm}$ are the asymmetry parameters of the respective tensors. Introducing the tensor components from (16) into (18) and (19) the following simple relations are obtained:

$$\delta^{\pm} = \mp\frac{3}{4}\frac{e^2qQ}{h}\tilde{\nu}^{\pm}(Z) \ , \tag{20}$$

$$\eta^{\pm} = \frac{\tilde{\nu}^{\pm}(Y) - \tilde{\nu}^{\pm}(X)}{\tilde{\nu}^{\pm}(Z)} \ . \tag{21}$$

IV. NMR Powder Patterns for Axially Symmetric Coupling Tensors

If the EFG and S tensors are both axially symmetric the formalism developed in Sect. III simplifies considerably. Besides $\eta_Q = \eta_S = 0$ the Eulerian angles α and γ can be chosen zero whence β is the angle between the distinct principle axes of the tensors under consideration. Under these circumstances (14) becomes

$$\frac{\nu_Q \pm \nu_S}{\frac{3}{4}\,\mathrm{QCC}} = \begin{pmatrix} -\frac{1}{2}\,[1 \pm A(1-3\sin^2\beta)] & 0 & -\frac{3}{4}\,A\sin 2\beta \\ 0 & -\frac{1}{2}\,(1 \pm A) & 0 \\ -\frac{3}{4}\,A\sin 2\beta & 0 & 1 \pm A(1-\frac{3}{2}\sin^2\beta) \end{pmatrix} . \tag{22}$$

The eigenvalues of (17) may easily be calculated as

$$\tilde{\nu}^{\pm}(1) = -\tfrac{1}{2}(1 \pm A) \ ,$$

$$\tilde{\nu}^{\pm}(2) = \tfrac{1}{4}(1 \pm A) + \tfrac{3}{4}\sqrt{A^2 \pm 2A(1-2\sin^2\beta)+1} \ ,$$

$$\tilde{\nu}^{\pm}(3) = -[\tilde{\nu}^{\pm}(1) + \tilde{\nu}^{\pm}(2)] \ , \tag{23}$$

from which the following most interesting relationship may be derived:

$$2(\tilde{\nu}^{\pm}(1))^2 + \tilde{\nu}^{\pm}(2)\,\tilde{\nu}^{\pm}(3) = \pm\tfrac{9}{4}A\sin^2\beta \ . \tag{24}$$

If one relables these eigenvalues according to the recipe given above, (16), and inserts them into (23),

Table 1. I_z-representation of the eight base operators.

$$L_x^{10} = \frac{1}{2}\begin{pmatrix} 0 & 1 & 0 \\ 1 & 0 & 0 \\ 0 & 0 & 0 \end{pmatrix} \qquad L_x^{0-1} = \frac{1}{2}\begin{pmatrix} 0 & 0 & 0 \\ 0 & 0 & 1 \\ 0 & 1 & 0 \end{pmatrix}$$

$$L_x^{1-1} = \frac{1}{2}\begin{pmatrix} 0 & 0 & 1 \\ 0 & 0 & 0 \\ 1 & 0 & 0 \end{pmatrix}$$

$$L_y^{10} = \frac{1}{2}\begin{pmatrix} 0 & -i & 0 \\ i & 0 & 0 \\ 0 & 0 & 0 \end{pmatrix} \qquad L_y^{0-1} = \frac{1}{2}\begin{pmatrix} 0 & 0 & 0 \\ 0 & 0 & -i \\ 0 & i & 0 \end{pmatrix}$$

$$L_y^{1-1} = \frac{1}{2}\begin{pmatrix} 0 & 0 & -i \\ 0 & 0 & 0 \\ i & 0 & 0 \end{pmatrix}$$

$$L_z^{10} = \frac{1}{3}\begin{pmatrix} 2 & 0 & 0 \\ 0 & -1 & 0 \\ 0 & 0 & -1 \end{pmatrix} \qquad L_z^{0-1} = \frac{1}{3}\begin{pmatrix} 1 & 0 & 0 \\ 0 & 1 & 0 \\ 0 & 0 & -2 \end{pmatrix}$$

Table 2. A and β values and tensor parameters characterizing the spectra shown in Figure 3.

No.	A	$\frac{\beta}{\text{deg}}$	$\frac{\delta^+}{(3/4)(e^2qQ/h)}$	η^+	$\frac{\delta^-}{(3/4)(e^2qQ/h)}$	η^-
3a	0	–	-1	0	1	0
3b	∞	–	$\left[\delta^+ = \frac{2}{3}\nu_z \Delta s\right]$	0	$\left[\delta^- = \frac{2}{3}\nu_z \Delta s\right]$	0
3c	0.15	0	-1.15	0	0.85	0
3d	0.15	90	-0.925	0.243	1.075	0.209

the powder spectrum can be calculated. Similarly, the tensor parameters $\delta^{\pm}$ and $\eta^{\pm}$ may be obtained with the use of (20) and (21).

Figure 3 shows several typical powder patterns which were calculated on the basis of (16) and (23) for various values of the parameters A and β. These values as well as the tensor parameters δ and η from (20) and (21) are collected in Table 2.

Figures 3, a and b, serve to check the internal consistency of the theoretical treatment in that they reproduce correctly the powder spectra of the axially symmetric EFG and S tensors introduced.

Figures 3, c and d, demonstrate the effect the change of the relative orientation of the EFG and S tensors from parallel ($\beta = 0°$) to perpendicular ($\beta = 90°$) has on the appearence of the powder spectrum for $A = 0.15$ (this value corresponds to the case: width of the pure shielding pattern $= 0.11 \times$ width of the pure quadrupole spectrum). Obviously, the spectra are quite different but the differences mainly show up in the outer spectral portions. The complete β-dependence of the powder pattern for $A = 0.15$ may be obtained from the δ and η parameters as function of β shown in Figure 4. It is evident that the $\beta = 0°$ and $\beta = 90°$ cases just represent the extreme cases of the powder spectrum appearance.

From a practical point of view the problem of most interest concerns the analysis of an experimentally determined powder spectrum in terms of the quadrupole coupling constant QCC, the shielding anisotropy Δs, and the angle β between the distinct principle axes of the two axially symmetric coupling tensors under consideration.

The type of functional dependence on β of the quantities $\tilde{\nu}^{\pm}$ given by (23) predicts identical spectra for angles β and $180°$-β which, consequently, allows the treatment to be restricted to β values in the range $0 \leqslant \beta \leqslant 90°$. For reasons of practical interest the discussion is limited to A values with $0 \leqslant |A| \leqslant 1$.

The first step of the analysis consists of the decomposition of a given powder spectrum into

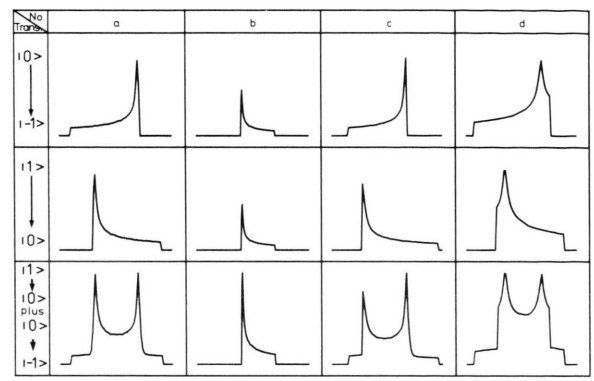

Fig. 3. Examples of calculated powder patterns in the case of axially symmetric electric field gradient and magnetic shielding tensors. The various cases refer to the A and β parameter values collected in Table 2. The frequency axis runs from right to left as in Figure 2.

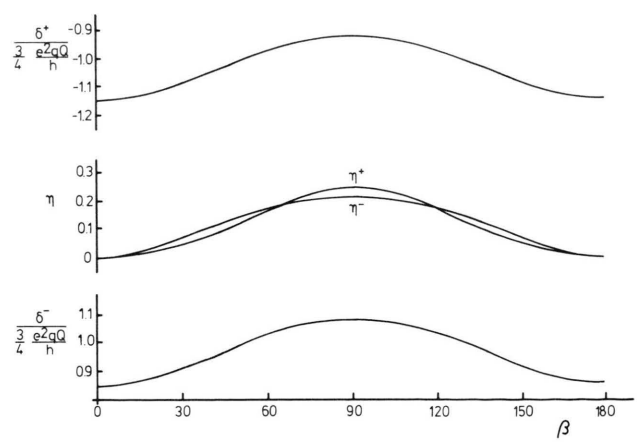

Fig. 4. Parameters δ and η characterizing the tensors ν_{10} and ν_{0-1} as functions of the angle β for $A = 0.15$.

the constituting subpatterns (Figure 2). This can always readily be accomplished by using the fact that the traces of the tensors $\mathbf{v}_{01}$ and $\mathbf{v}_{0-1}$ are identical and equal to ν_0. Because of the a priori unknown signs of QCC and Δs the correspondence between the subpatterns and the transitions $|1\rangle \rightarrow |0\rangle$ and $|0\rangle \rightarrow |-1\rangle$ cannot immediately be established. Therefore, in the discussion to follow the various cases with respect to the signs of QCC and Δs are considered separately. For reasons of easy parlance a subpattern having its Z edge on the high frequency (HF) side of ν_0 (left hand side according to the conventional use adopted here) is termed α type. A subpattern having its Z edge to lower frequencies (LF) than ν_0 is termed ζ type.

Case (i): QCC > 0, $\Delta s \geqslant 0$, $0 \leqslant A \leqslant 1$. Under these circumstances (16) and (23) yield the following relations: $\nu_{0-1}(2) \geqslant \nu_0 > \nu_{0-1}(1) \geqslant \nu_{0-1}(3)$, whence $\nu_{0-1}(2) = \nu_{0-1}(Z)$, $\nu_{0-1}(1) = \nu_{0-1}(Y)$, and $\nu_{0-1}(3) = \nu_{0-1}(X)$. Thus, the subpattern belonging to the $|0\rangle \rightarrow |-1\rangle$ transition is α type (Figure 2). – $\nu_{10}(1) \geqslant \nu_0 \geqslant \nu_{10}(2)$ and $\nu_{10}(1) \geqslant \nu_{10}(3) \geqslant \nu_{10}(2)$, whence $\nu_{10}(3) = \nu_{10}(Y)$. Since $\nu_{10}(Y)$ representing the singularity of the subpattern (the peak in the case of finite individual linewidths) may appear on either side of ν_0 (depending on the values of A and β), the $|1\rangle \geqslant \rightarrow |0\rangle \geqslant$ transition subpattern is of ζ type if $\nu_{10}(Y) \geqslant \nu_0$, then $\nu_{10}(1) = \nu_{10}(X)$ and $\nu_{10}(2) = \nu_{10}(Z)$, or is of α type if $\nu_{10}(Y) \leqslant \nu_0$, then $\nu_{10}(1) = \nu_{10}(Z)$ and $\nu_{10}(2) = \nu_{10}(X)$. The values of A and β for which these two different cases are realized are located within the regions I and II of the A-β reactangle shown in Figure 5. The border curve **a** along which $\nu_{10}(Y) = \nu_0$ is represented by the equation $\sin^2\beta = 2(1+A)^2/9A$.

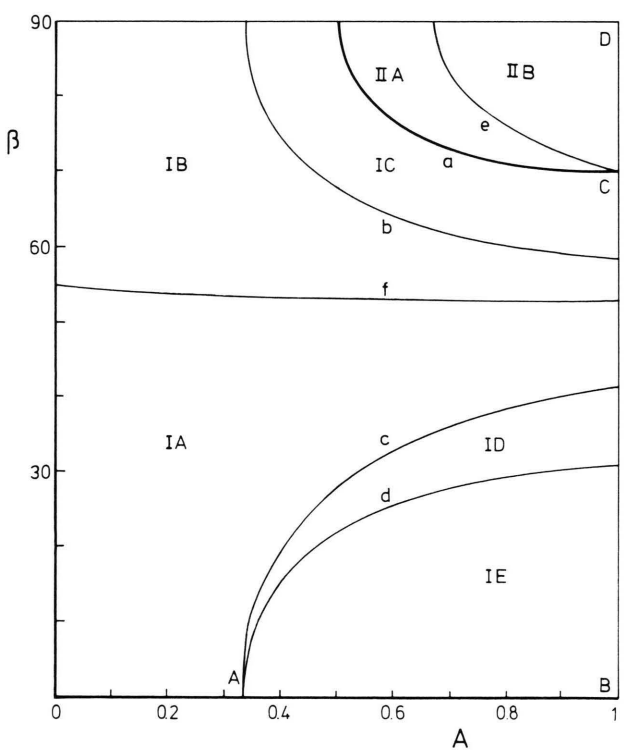

Fig. 5. A-β coordinate rectangle being partitioned by the curves **a** to **f** into the main regions I and II as well as the subregions IA to IE, IIA and IIB. The curves **a** to **f** obey the following equations. Curve **a**: $\sin^2\beta = 2(1+A)^2/9A$; curve **b**: $\sin^2\beta = (1/2) + (1/18A)\sqrt{9A^2+8}$; curve **c**: $\sin^2\beta = (1/9A)(6A-2)$; curve **d**: $\sin^2\beta = (1/2) - (1/18A)\sqrt{9A^2+8}$; curve **e**: $\sin^2\beta = (1/9A) \cdot (6A+2)$; curve **f**: $\sin^2\beta = (1/25A)(-3A^2+14A-3+(1+A)\sqrt{9A^2-2A+9})$.

For (A, β) in region I, where the α-ζ subpattern pair case is realized the physical parameters QCC, A, and β, may be evaluated from the distinct frequencies of the edges and singularities (Fig. 6) as follows:

$$
\begin{aligned}
&① \quad \nu^{\zeta}(X) - \nu^{\alpha}(Y) = \tfrac{3}{4}|\mathrm{QCC}|\,, \\
&② \quad \nu^{\zeta}(X) - \nu_0 \quad\;\; = \tfrac{3}{8}|\mathrm{QCC}|(1+|A|)\,, \\
&③ \quad \nu^{\alpha}(Z) - \nu^{\alpha}(X) \qquad\qquad (25) \\
&\qquad = \tfrac{9}{8}|\mathrm{QCC}|\sqrt{(1+|A|)^2 - 4|A|\cos^2\beta}\,, \\
&④ \quad \nu^{\zeta}(Y) - \nu^{\zeta}(Z) \\
&\qquad = \tfrac{9}{8}|\mathrm{QCC}|\sqrt{(1+|A|)^2 - 4|A|\sin^2\beta}\,.
\end{aligned}
$$

In these equations the moduli of A and QCC have been introduced in order to allow easy reference in

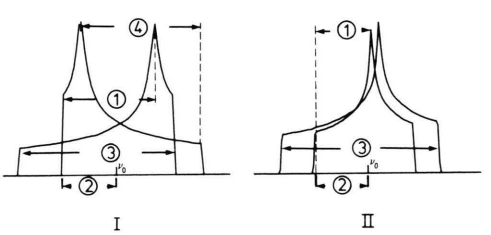

Fig. 6. The basic types of subpattern pairs for values of (A, β) in regions I and II of Figure 5. The encircled numbers denote the distinct frequency separations according to (25) and (26). The frequency axis runs from right to left as in Figure 2.

connection with the negative sign cases to be discussed below. The equations denoted ③ and ④ in (25) are to be considered as alternatives for the evaluation of β.

For (A, β) in region II, where both subpatterns are of the α type, the following relations may be used to evaluate the parameters QCC, A, and β (Figure 6):

$$\begin{aligned} &① \quad \nu^{\alpha'}(Z) - \nu^{\alpha}(Y) = \tfrac{3}{4}|\mathrm{QCC}|\,, \\ &② \quad \nu^{\alpha'}(Z) - \nu_0 \quad\;\; = \tfrac{3}{8}|\mathrm{QCC}|(1+|A|)\,, \\ &③ \quad \nu^{\alpha}(Z) - \nu^{\alpha}(X) \\ &\qquad = \tfrac{9}{8}|\mathrm{QCC}|\sqrt{(1+|A|)^2 - 4|A|\cos^2\beta}\,. \end{aligned} \tag{26}$$

The indices α and α' refer to the subpatterns having the Z edges at the outermost left side and next to ν_0, respectively. The inherent relation $\nu^{\alpha'}(Z) < \nu^{\alpha}(Z)$ or, equivalently, $\nu_{10}(Z) < \nu_{0-1}(Z)$ follows from (16) and (23).

The internal consistency of the analysis just described may be checked with the aid of (24), which in terms of the distinct subpattern frequencies reads

$$\begin{aligned} &2|\nu^{\alpha}(Y) - \nu_0|^2 - |\nu^{\alpha}(Z) - \nu_0||\nu^{\alpha}(X) - \nu_0| \\ &= -\frac{81}{64}(\mathrm{QCC})^2|A|\sin^2\beta\,, \\ &2|\nu^{\zeta}(X) - \nu_0|^2 - |\nu^{\zeta}(Z) - \nu_0||\nu^{\zeta}(Y) - \nu_0| \\ &= \frac{81}{64}(\mathrm{QCC})^2|A|\sin^2\beta \quad \text{for region I, and} \end{aligned} \tag{27}$$

$$\begin{aligned} &2|\nu^{\alpha}(Y) - \nu_0|^2 - |\nu^{\alpha}(Z) - \nu_0||\nu^{\alpha}(X) - \nu_0| \\ &= -\frac{81}{64}(\mathrm{QCC})^2|A|\sin^2\beta\,, \\ &2|\nu^{\alpha'}(Z) - \nu_0|^2 - |\nu^{\alpha'}(X) - \nu_0||\nu^{\alpha'}(Y) - \nu_0| \\ &= \frac{81}{64}(\mathrm{QCC})^2|A|\sin^2\beta \quad \text{for region II}\,. \end{aligned} \tag{28}$$

A look at Fig. 6 immediately puts the question whether under certain circumstances, i.e. for certain values of A and β, there are coincidences between the edges and singularities of the subpatterns. In fact, of the eight coincidences conceivable (4 for each region) a total of four does occur for (A, β) points being located on the curves **b** to **e** in the A-β rectangle (Figure 5). These coincidences are for region I of the LF edges (curve **b**), of the HF edges (curve **c**), of the HF edge and HF singularity (curve **d**), and for region II of the singularities (curve **e**). Most conveniently, a further curve **f** is drawn in region I of Fig. 5 along which the corresponding subpatterns exhibit the same edge separation on both sides of ν_0. Interestingly, this feature of the subpatterns is realized for β values near the magic angle.

The curves **b** to **f** just introduced partition the regions I and II of Fig. 5 into subregions IA to IE, IIA and IIB, where the subpattern edges and singularities have characteristic positions relative to each other. Subpattern pairs for typical (A, β) points from inside these subregions are displayed in Figure 7.

For (A, β) in subregions IA and IB the powder spectra are terminated on both sides of ν_0 by edges of the Z type. In IA the separation between the X and Z edges is larger on the LF side of ν_0 than on the HF side, whereas the reverse situation holds true in IB.

For (A, β) in IC on both sides of ν_0 the Z edge is to the left of the X edge of the alternate pattern whereas the reverse situation is realized in ID and IE. The characteristic difference of the patterns belonging to ID and IE is the position of the HF side Z edge which is between the X edge and Y singularity and between the Y singularity and ν_0, respectively.

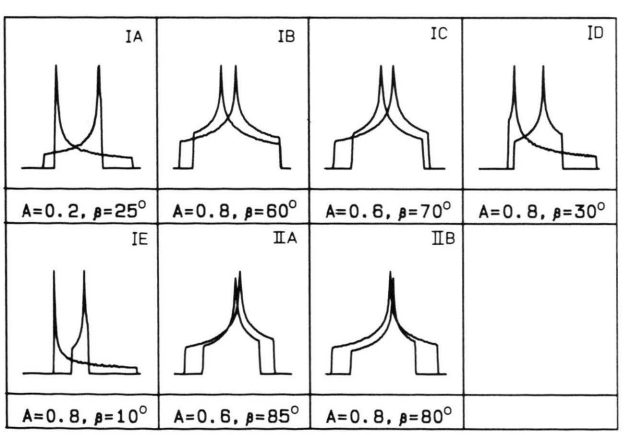

Fig. 7. Simulated subpattern pairs for values of A and β in the subregions IA to IE, IIA and IIB of Figure 5. The frequency axis runs from right to left as in Figure 2.

The patterns belonging to (A, β) in subregions IIA and IIB have the singularity of the subpattern with the Z edge at the extreme left to higher and lower frequency, respectively, of the singularity of the alternate subpattern.

For (A, β) along the A and β coordinate axes (Fig. 5) both subpatterns come from axially symmetric ν_{10} and ν_{0-1} tensors, therefore showing up each one edge and one singularity only. Along $A = 1$ (as well as along curve **a**) one pattern is of the $\eta = 1$ type.

It seems worthwhile to display the patterns for four distinct points (A, β) denoted by A to D in Fig. 5 for which quite unusual powder patterns appear (Figure 8). In A the HF edge and singularity of two axially symmetric tensor subpatterns coincide so that the resulting powder pattern exhibits one edge only and two singularities. In B a single line (ideally a δ function) at ν_0 appears superimposed on an axially symmetric tensor subpattern. In C both subpatterns are of the $\eta = 1$ type, whereas in D an $\eta = 0$ and $\eta = 1$ subpattern combination is realized.

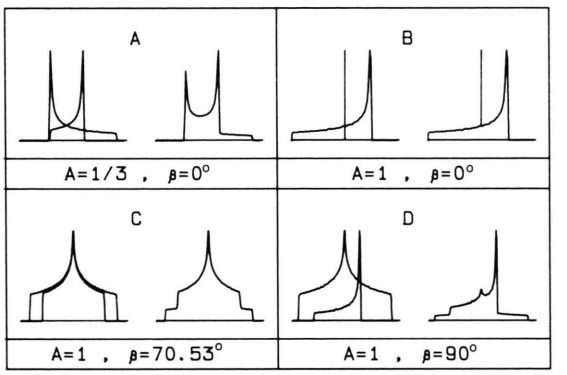

Fig. 8. Simulated subpattern pairs and resulting powder spectra for the points A to D denoted in Figure 5. The frequency axis runs from right to left as in Figure 2.

Case (ii): QCC <0, $\Delta s \geqslant 0$, $-1 \leqslant A \leqslant 0$. A careful analysis of (16) and (23) reveals that in comparison to case (i) identical subpatterns appear, but with the assignments to the transitions $|1\rangle \rightarrow |0\rangle$ and $|0\rangle \rightarrow |-1\rangle$ interchanged. This entails that the same procedure of analysis of the subpattern pairs as described previously may be applied giving the moduli of QCC and A. As expected, the sign of QCC cannot be deduced from the powder spectra.

Case (iii). QCC <0, $\Delta s \leqslant 0$, $0 \leqslant A \leqslant 1$. Equation (16) tells that in comparison to case (i) the subpatterns appear mirrored at the vertical line passing through ν_0. Since the mirror images of spectra with values of (A, β) in region II and in subregion ID have no analogues anywhere in the A-β rectangle (Fig. 7), case (iii) spectra can readily be distinguished from those discussed previously. The moduli of QCC and A are, therefore, obtained by mirroring the subpatterns at ν_0 and subsequently applying the procedure of analysis described previously.

The mirror images of the patterns which originate from (A, β) values in subregions IA and IC exhibit the characteristics of the patterns resulting from (A, β) values in subregions IB and IE, respectively, and vice versa. Therefore it cannot readily be decided from the characteristic positions of the edges whether, for instance, a given subpattern pair with the characteristic features of subregion IA is case (i) or (ii) with (A, β) in IA, or is case (iii), i.e. the mirror image of a pattern pair with (A, β) in IB.

This apparent ambiguity can, however, easily be resolved with the aid of (27). Since the X and Y principle axis frequencies enter into the equations for the α and ζ subpatterns in a different way, these equations can, obviously, after mirroring only be fulfilled if α and ζ are interchanged, too. Thus, if a case (iii) situation is given, but the pattern analysis is performed according to the procedure described previously the conditions imposed by (27) cannot be fulfilled unless $A = 0$. Consequently, if (27) does not hold true, it is known that $\Delta s \leqslant 0$, and the moduli of QCC and A as well as β are obtained by applying the previously described procedure after having performed the mirroring at ν_0.

Case (iv): QCC >0, $\Delta s \leqslant 0$, $-1 \leqslant A \leqslant 0$. In comparison to case (iii) the sign of QCC is changed. Referring to the reasoning under case (ii) there is no change in the spectral appearance in comparison to case (iii) just discussed.

The foregoing results are of great interest for the interpretation of deuteron solid state NMR spectra of molecules adsorbed on the basal planes of microcrystalline graphite substrates. As a matter

of fact, for deuterons in molecules of diamagnetic solids where the shielding tensor is mainly intramolecular in origin (chemical shielding) the shielding contribution is practically negligible in comparison to the quadrupole coupling. For typical values of the proton chemical shielding anisotropy [7], $\Delta\sigma = 25$ ppm, and of the deuterium quadrupole coupling constant, $e^2qQ/h =$ 160 kHz [7], the value of A is 0.008 in a Zeeman field of 8.5 T ($\nu_Z = 55$ MHz). In addition, in the case of rapid anisotropic rotations of the molecules the EFG and chemical shielding tensors, are, in general, averaged simultaneously since both are fixed with respect to the molecular framework.

The situation is very much different for adsorption with graphite as the solid support. In this case the shielding tensor has a shielding anisotropy Δs in range 150 to 200 ppm [1, 9] and can be assumed to be axially symmetric with the distinct principle axis normal to the graphite basal planes [1, 9]. With $\Delta s = 150$ ppm, $e^2qQ/h = 160$ kHz, and $\nu_Z = 55$ MHz the parameter A comes out as 0.05.

Much larger values of A result if some anisotropic rotational motions of the adsorbed molecules proceed rapidly on the NMR time scale. Under these circumstances the rigid EFG tensor is averaged to a new tensor with, in general, reduced apparent quadrupole coupling constant. For a deuteron in a rapidly rotating methyl group, for instance, the averaged tensor is axially symmetric with the distinct principal axis aligned along the rotation axis, and has an apparent quadrupole coupling constant which is the negative one third of the rigid value [10, 11]. Under these circumstances QCC in (15) and (16) refers to the averaged EFG tensor, and β now denotes the angle between the averaged EFG tensor and the S tensor distinct principle axes. Consequently, $A = 0.15$ for this case since the shielding tensor remains unaffected by the molecular rotational motion. Actually, ^{2}H spectra with $A = 0.15$, $\beta = 90°$ and $A = 0.30$, $\beta = 0°$ have recently been measured in our laboratory with p-xylene ($C_6H_4(CD_3)_2$) and toluene (C_7D_8), respectively, adsorbed on graphitized carbon black [12]. Further examples with benzene adsorbed on the graphitized blacks Graphon ($A = 0.075$, $\beta = 0°$) and Sterling MT ($A = 0.101$, $\beta = 0°$) have recently been published [1].

Of special interest in such studies is the angle β. Since, by definition, β determines the orientation of the S tensor, which is fixed within the graphite substrate, relative to the EFG tensor, either rigid or averaged, which is fixed within the framework of the adsorbed molecule, the orientation of the molecule with respect to the surface can easily be deduced.

V. Conclusions

A conceptually simple formalism has been developed which allows to carry out conveniently the calculation of spin $I = 1$ powder patterns if the nuclei are subject to both quadrupole and shielding interactions. Although such twofold interactions are usually not encountered in bulk phases, it seems nevertheless worthwhile to reexamine the quadrupole coupling constants and, especially, the asymmetry parameters of deuterium reported in the literature for such phases. This remark refers less to solid state powder studies but to single crystal and aligned molecules in liquid crystal investigations where the Pake doublet line splitting might perceptibly be influenced by tensorial interactions other than quadrupole, e.g. by chemical shielding anisotropy.

Acknowledgements

Support of this work by Deutsche Forschungsgemeinschaft is gratefully acknowledged.

[1] B. Boddenberg and R. Grosse, Z. Naturforsch. **41a**, 1361 (1986).
[2] D. J. Siminovitch, M. Rance, K. R. Jeffrey, and M. F. Brown, J. Magn. Res. **58**, 62 (1984).
[3] U. Fano, Rev. Mod. Phys. **29**, 74 (1957).
[4] A. Wokaun and R. R. Ernst, J. Chem. Phys. **67**, 1752 (1977).
[5] H. W. Spiess, in: "NMR. Basic Principles and Progress", edited by P. Diehl, E. Fluck, and R. Kosfeld, Springer, Berlin 1978, Vol. 15, p. 55.
[6] M. H. Cohen and R. Reif, in: "Solid State Physics", edited by F. Seitz and D. Turbull, Academic Press, New York 1957, Vol. 5, p. 321.
[7] U. Haeberlen, in: "Advances in Magnetic Resonance", edited by J. S. Waugh, Academic Press, New York 1976, Suppl. 1, p. 1.
[8] H. H. Mantsch, H. Saito, and I. C. P. Smith, Progr. NMR Spectrosc. **11**, 211 (1977).
[9] G. Neue, Dissertation, University of Dortmund, 1983.
[10] R. G. Barnes, in: "Advances in Nuclear Quadrupole Resonance", edited by J. A. S. Smith, Heyden, London, Vol. 1, p. 335.
[11] B. Boddenberg, in: "Lectures on Surface Science", edited by G. R. Castro and M. Cardona, Springer, Berlin 1987, p. 226.
[12] B. Boddenberg and R. Grosse, to be published.